ExoMol line lists – XXXIX. Ro-vibrational molecular line list for CO_2

S. N. Yurchenko[1], Thomas M. Mellor[1], Richard S. Freedman[2,3] and J. Tennyson[1]⋆

[1]*Department of Physics and Astronomy, University College London, Gower Street, WC1E 6BT London, UK;*
[2]*NASA Ames Research Center, Mail Stop 245-3, Moffett Field, CA 94035-1000, USA;*
[3] *SETI Institute, Mountain View, CA, USA.*

10 July 2020

ABSTRACT

A new hot line list for the main isotopologue of CO_2, $^{12}C^{16}O_2$ is presented. The line list consists of almost 2.5 billion transitions between 3.5 million rotation-vibration states of CO_2 in its ground electronic state, covering the wavenumber range 0–$20\,000$ cm^{-1} ($\lambda > 0.5\,\mu$m) with the upper and lower energy thresholds of $36\,000$ cm^{-1} and $16\,000$ cm^{-1}, respectively. The ro-vibrational energies and wavefunctions are computed variationally using the Ames-2 accurate empirical potential energy surface. The ro-vibrational transition probabilities in the form of Einstein coefficients are computed using an accurate *ab initio* dipole moment surface using variational program TROVE. A new implementation of TROVE which uses an exact nuclear-motion kinetic energy operator is employed. Comparisons with the existing hot line lists are presented. The line list should be useful for atmospheric retrievals of exoplanets and cool stars. The UCL-4000 line list is available from the CDS and ExoMol databases.

Key words: molecular data: Physical data and processes; planets and satellites: atmospheres; planets and satellites: gaseous planets; infrared: general; stars: atmospheres.

1 INTRODUCTION

Carbon dioxide is well-known and much studied constituent of the Earth's atmosphere. However, it is also an important constituent of planetary atmospheres. The Venusian atmosphere is 95% CO_2 which therefore dominates its opacity (Snels et al. 2014). Similarly studies of exoplanets have emphasised the importance of CO_2. It was one of the first molecules detected in the atmospheres of hot Jupiter exoplanets (Swain et al. 2009a,b, 2010) where it provides an important measure of the C/O ratio on the planet (Moses et al. 2013). Similarly it is considered an important marker in directly imaged exoplanets (Moses et al. 2013) and the atmospheres of lower mass planets are expected to be dominated by water and CO_2 (Massol et al. 2016). Heng & Lyons (2016) provide a comprehensive study of CO_2 abundances in exoplanets. Recently, Baylis-Aguirre et al. (2020) detected emission and absorption from excited vibrational bands of CO_2 in the mid-infrared spectra of the M-type Mira variable R Tri using the Spitzer infrared spectrograph (IRS).

Most of the environments discussed above are considerably hotter then the Earth: for example Venus is at about 735 K and hot Jupiter exoplanets have typical atmospheric temperatures in excess of 1000 K. Hot CO_2 is also important for industrial applications on Earth (Evseev et al. 2012) and studies of combustion engines (Rein & Sanders 2010). These applications all require information on CO_2 spectra at higher temperatures. It is this problem that we address here.

The importance of CO_2 has led to very significant activity on the construction of list of important rotation-vibration transition lines. The HITRAN data base provides such lists for studies of the Earth's atmosphere and other applications at or below 300 K. The CO_2 line lists where comprehensively updated in the 2016 release of HITRAN (Gordon & et al. 2017)

⋆ The corresponding author: j.tennyson@ucl.ac.uk

in part to provide higher accuracy data to meet the demands of Earth observation satellites such as OCO-2 (Connor et al. 2016; Oyafuso et al. 2017). The 2016 update made extensive use of variational nuclear motion calculations (Zak et al. 2016, 2017b,a) of the type employed here.

HITRAN is not designed for or suitable for high temperature applications which demand much more extensive line lists. The HITEMP data base (Rothman et al. 2010) is designed to address this issue. The original HITEMP used the direct numerical diagonalization calculations of Wattson & Rothman (1992), which were an early example of the use of large scale variational nuclear motion calculations to provide molecular line lists. The 2010 HITEMP update used the CDSD-1000 (carbon dioxide spectroscopic databank) line list (Tashkun et al. 2003). The CDSD-1000 line list is based on the use effective Hamiltonian fits to experimental data and was designed to be complete for temperatures up to 1000 K. CDSD-1000 subsequently was replaced by CDSD-4000. The empirical CO_2 line list CDSD-4000 computed by Tashkun & Perevalov (2011) is designed for temperatures up to 5000 K, but has limited wavenumber coverage. Furthermore, while usually good at reproducing known spectra, experience has shown that the effective Hamiltonian approach can struggle to capture all the unobserved hot bands resulting in underestimates of the opacity at higher temperatures (Chubb et al. 2020). A compact version of CDSD-4000 has recently been made available (Vargas et al. 2020).

The NASA Ames group have produced a number of CO_2 line lists (Huang et al. 2013, 2014, 2017, 2019) using highly accurate potential energy surfaces (Huang et al. 2012, 2017) and variational nuclear motion calculations. Most relevant for this work is the Ames-2016 CO_2 line list of Huang et al. (2017) which considers wavenumbers up to 15 000 cm^{-1} and J up to 150 with upper state energies limited to $hc \times 24$ 000 cm^{-1}. Due to this fixed upper energy cut-off, the temperature coverage depends on the wavenumber range, from $T \sim 4000$ K at lower end up to ~ 1500 K at the higher end. The Ames-2016 line list was based on an accurate empirically-generated potential energy (PES) surface Ames-2 and their high-level *ab initio* dipole moment surface (DMS) DMS-N2.

High accuracy room temperature line lists for 13 isotopologues of CO_2 was computed by Zak et al. (2016, 2017b,a), using the Ames-2 PES (Huang et al. 2017) and UCL's highly accurate DMS (Polyansky et al. 2015). These line lists are now part of the HITRAN (Gordon & et al. 2017) and ExoMol (Tennyson & Yurchenko 2012) databases. The room temperature properties of this line list have been subject to a number experimental tests and the results have been found to be competitive in accuracy to state-of-the-art laboratory experiments (Odintsova et al. 2017; Kang et al. 2018; Čermák et al. 2018; Long et al. 2020).

Here we present a new hot line list for the main isotopologue of CO_2 ($^{12}C^{16}O_2$) generated using UCL's *ab initio* DMS (Polyansky et al. 2015) and the empirical PES Ames-2 (Huang et al. 2017) with the variational program TROVE (Yurchenko et al. 2007). Our line list is the most comprehensive (complete and accurate) data set for CO_2. This work is performed as part of the ExoMol project (Tennyson & Yurchenko 2012) and the results form an important addition to the ExoMol database (Tennyson et al. 2016) which, as discussed below, is currently being upgraded (Tennyson et al. 2020).

2 TROVE SPECIFICATIONS

For this work we used a new implementation of the exact kinetic energy (EKE) operator for triatomics in TROVE (Yurchenko & Mellor 2020) based on the bisector embedding for triatomic molecules (Carter et al. 1983; Sutcliffe & Tennyson 1991).

The variational TROVE program (Yurchenko et al. 2007) solves the ro-vibrational Schrödinger equation using a multi-layer contraction scheme (see, for example, Yurchenko et al. (2017)). At step 1, the 1D primitive basis set functions $\phi_{v_1}(r_1)$, $\phi_{v_2}(r_2)$ (stretching) and $\phi_{v_3}(\rho)$ (bending) are obtained by numerically solving the corresponding Schrödinger equations. Here r_1 and r_2 are two stretching valence coordinates and $\rho = 180° - \alpha$ with α being the inter-bond valence angle. A 1D Hamiltonian operator for a given mode is constructed by setting all other degrees of freedom to the their equilibrium values. The two equivalent stretching equations are solved on a grid of 1000 points using the Numerov-Cooley approach (Noumerov 1924; Cooley 1961), with the grid values of r_i ranging from $r_e - 0.4$ to $r_e + 1.0$ Å. The bending mode solutions are obtained on the basis of the associated Laguerre polynomials as given by

$$\phi_{n,l}^{(l)}(\rho) = C_{n,l}\, \rho^{l+1/2}\, L_n^{(l)}(a\rho^2)\, e^{-a\rho^2/2}, \tag{1}$$

normalized as

$$\int_0^{\rho_{\max}} \phi_{n,l}^{(l)}(\rho)^2\, d\rho = 1,$$

where a is a structural parameter, $l \geqslant 0$, $\rho_{\max}$ was set to $170°$ and all primitive bending functions were mapped on a grid of 3000 points. The kinetic energy operator is constructed numerically as a formal expansion in terms of the inverse powers of the stretching coordinates r_i ($i = 1, 2$): $1/r_i$ and $1/r_i^2$ around a non-rigid configuration (Hougen et al. 1970) defined by the ρ_i points on the grid. The singularities of the kinetic energy operator at $\rho = 0°$ ($\sim 1/\rho$ and $1/\rho^2$) are resolved analytically with the help of the factors $\rho^{l+1/2}$ in the definition of the associated Laguerre basis set in Eq. (1). The details of the model will be published elsewhere (Yurchenko & Mellor 2020).

At step 2 two reduced problems for the 2D stretching and 1D bending reduced Hamiltonians are solved variationally on the primitive basis set of $|v_1, v_2\rangle = \phi_{v_1}(r_1)\phi_{v_2}(r_2)$ and $|v_3, l\rangle = \phi_{v_3}^{(l)}(\rho)$, respectively. The reduced Hamiltonians are constructed by averaging the 3D vibrational ($J = 0$) Hamiltonian over the ground state basis functions as follows:

$$\hat{H}_{\mathrm{str}}^{(1)}(r_1, r_2) = \langle 0_3, l = 0|\hat{H}^{\mathrm{3D}}|0_3, l = 0\rangle, \tag{2}$$

$$\hat{H}_{\mathrm{bnd}}^{(2)}(\rho) = \langle 0_1, 0_2|\hat{H}^{\mathrm{3D}}|0_1, 0_2\rangle, \tag{3}$$

where $|v_1, v_2\rangle$ are stretching and $|v_3, l\rangle$ are bending vibrational basis functions with $v_i = 0$ and $l = 0$. In the bending basis set, l is treated as a parameter with the corresponding Hamiltonian matrices

$$H_{i,j}^{(2),l} = \langle i, l|\hat{H}_{\mathrm{bnd}}^{(2)}(\rho)|j, l\rangle,$$

block-diagonal in l ($l = 0, \ldots, l_{\max}$). The eigenfunctions of the reduced Hamiltonians in Eqs. (2,3), $\Phi_{i_1}^{(1)}(r_1, r_2)$ and $\Phi_{i_2,l}^{(2)}(\rho)$ are obtained variationally and then symmetrized using the automatic symmetry adaptation technique (Yurchenko et al. 2017). A 3D vibrational basis set for the $J = 0$ Hamiltonian for step 3 is then formed as symmetry adapted products given by:

$$\Phi_{i_1,i_2,l}^{\Gamma_{\mathrm{vib}}} = \{\Phi_{i_1}^{(1)}(r_1, r_2)\,\Phi_{i_2,l}^{(2)}(\rho)\}^{\Gamma_{\mathrm{vib}}}, \tag{4}$$

where Γ_{vib} is the vibrational symmetry in the $\mathcal{C}_{2\mathrm{v}}(\mathrm{M})$ molecular symmetry group (Bunker & Jensen 1998) used to classify the irreducible representations (irreps) of the ro-vibrational states of CO$_2$. $\mathcal{C}_{2\mathrm{v}}(\mathrm{M})$ comprises four irreps A_1, A_2, B_1 and B_2. The allowed vibrational symmetries are A_1 and B_2. The allowed ro-vibrational symmetries of $^{12}\mathrm{C}^{16}\mathrm{O}_2$ are A_1 and A_2 due to the restriction on the nuclear-spin-ro-vibrational functions imposed by the nuclear spin statistics (Pauli exclusion principle).

At step 3, the vibrational ($J = 0$) Hamiltonians are solved on the symmetry adapted vibrational basis in Eq. (4). These eigenfunction $\Psi_{\lambda,l}^{(J=0)}$ are parameterized with l and associated with a vibrational symmetry A_1 or B_2 and then used to build a ro-vibrational basis set ($J \geqslant 0$) as a symmetrized product:

$$\Psi_{\lambda,K}^{(J,\Gamma)} = \{\Psi_{\lambda,K}^{(J=0,\Gamma_{\mathrm{vib}})}\,|J, K, \Gamma_{\mathrm{rot}}\rangle\}^{\Gamma}, \tag{5}$$

where the rotational part $|J, K, \Gamma_{\mathrm{rot}}\rangle$ is a symmetrized combination of the rigid rotor functions (Yurchenko et al. 2017) and the rotational quantum number K ($K \geqslant 0$) is constrained to the vibrational parameter l ($K = l$).

An $E = hc \times 36\,000$ cm^{-1} energy cut-off was used to contract the $J = 0$ eigenfunctions. All energies and eigenfunctions up to $J = 202$ were generated and used to produce the dipole lists for CO$_2$.

The size of the vibrational basis was controlled by a polyad-number condition:

$$P = v_1 + v_2 + v_3 \leqslant P_{\max} = 64,$$

chosen based on the convergence tests with v_1 and $v_2 \leqslant 56$.

Some vibrational energies computed using the Ames-2 PES by Huang et al. (2017) are shown in Table 1 and compared to the empirical $^{12}\mathrm{C}^{16}\mathrm{O}_2$ band centres (HITRAN's estimates, see below). In order to improve the accuracy of the ro-vibrational energies, we have applied vibrational band centre corrections to the TROVE $J = 0$ energies by shifting them to the HITRAN values, where available (see Yurchenko et al. (2011)). This trick in combination with the $J = 0$ contracted basis set allowed us to replace the diagonal vibrational matrix elements in the ro-vibrational Hamiltonian by the corresponding empirical band centres; for this reason the approach was named by Yurchenko et al. (2011) the empirical basis set correction (EBSC). The band centre corrections were estimated as average residuals $\tilde{E}_i^{\mathrm{T}} - \tilde{E}_i^{\mathrm{H}}$ ($J = 0, \ldots, 40$) by matching the TROVE $\tilde{E}_i^{\mathrm{T}}$ and HITRAN $\tilde{E}_i^{\mathrm{H}}$ ro-vibrational term values for $J \leqslant 40$, wherever available, for each vibrational state present in HITRAN. In total, 337 band centres[1] ranging up to $\sim 15\,500$ cm^{-1} were corrected, with the total root-mean-square (rms) error of 0.06 cm^{-1}. This is illustrated in Table 1, where 60 lowest term values before and after correction are shown together with the three alternative assignment cases, and in Fig. 1, where the average ro-vibrational errors for 337 bands are plotted. The complete list of the band centres and their corrections is given as supplementary material to the paper.
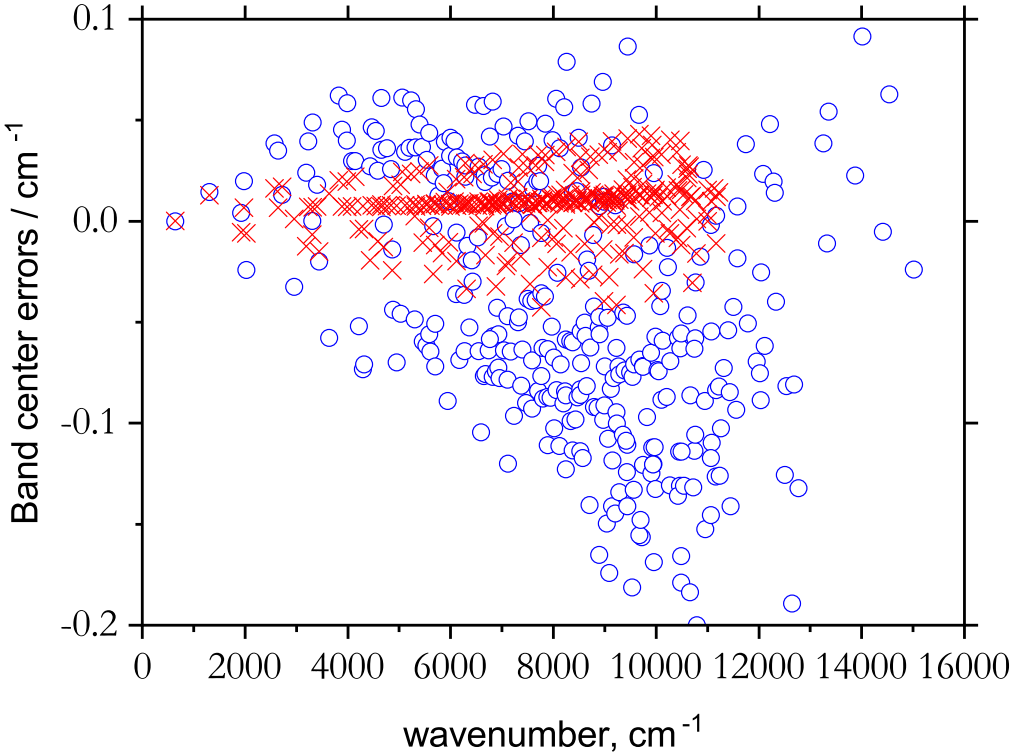
As an independent benchmark of the TROVE calculations, the initial TROVE energies ($J \leqslant 40$) before the band centre corrections were compared to the theoretical CO$_2$ energies computed by Zak et al. (2016) using the DVR3D program (Tennyson et al. 2004) and the same PES as the Ames-2016 line list. Figure 1 shows averaged residuals for 294 bands matched to the CO$_2$ energy term values from Zak et al. (2016) up to 10 500 cm^{-1} with the total rms error of 0.02 cm^{-1}.

The ro-vibrational energies were computed variationally using the CO$_2$ empirical PES Ames-2 by Huang et al. (2017) for $J = 0 \ldots 230$ and used for the temperature partition function of CO$_2$. The transitional intensities (Einstein A coefficients) were then computed using the UCL *ab initio* DMS (Polyansky et al. 2015) covering the wavenumber range from 0 to 20 000 cm^{-1} with the lower energy term value up to 16 000 cm^{-1} ($J \leqslant 202$). To speed up the calculation of the dipole moment matrix elements, a threshold of 10^{-12} to the eigen-coefficients was applied (see Yurchenko et al. (2011)). We have also applied a threshold of 10^{-8} Debye to the vibrational matrix elements of the dipole moment in order to reduce an accumulation error for higher overtones, see discussion by Medvedev et al. (2016, 2020).

---

[1] The band centres in question correspond to the fundamental or overtone bands and represent pure vibrational ($J = 0$) term values.

Table 1. Examples of vibrational band centres of CO_2 computed using Ames-2 PES with TROVE ($\tilde{E}_\lambda^{\mathrm{T}}$), average differences with the HITRAN band centres ($\Delta \tilde{E}_\lambda = \tilde{E}_\lambda^{\mathrm{H}} - \tilde{E}_\lambda^{\mathrm{T}}$), the shifted band canters adopted for ro-vibrational calculations ($\tilde{E}_\lambda^{\mathrm{T}} + \Delta \tilde{E}_\lambda$) and three sets of quantum numbers (QN) used in this work. See the complete table in supplementary material.

|	Linear Molecule QN				HITRAN QN					TROVE QN			Term values (cm^{-1})		
λ	n_1	n_2^{lin}	l_2	n_3	m_1	m_2	l_2	m_3	r	v_1	v_2	v_3	$\tilde{E}_\lambda^{\mathrm{T}}$	$\Delta \tilde{E}_\lambda$	$\tilde{E}_\lambda^{\mathrm{T}} + \Delta \tilde{E}_\lambda$
1	0	0	0	0	0	0	0	0	1	0	0	0	0.000	0.000	0.000
2	0	1	1	0	0	1	1	0	1	0	0	0	667.755	0.015	667.769
3	0	2	0	0	1	0	0	0	2	0	0	1	1285.404	0.004	1285.408
4	0	2	2	0	0	2	2	0	1	0	0	0	1336.673	0.020	1336.693
5	1	0	0	0	1	0	0	0	1	1	0	0	1388.209	-0.024	1388.185
6	0	3	1	0	1	1	1	0	2	0	0	1	1932.821	0.039	1932.860
7	0	3	3	0	0	3	3	0	1	0	0	0	2006.732	0.035	2006.766
8	1	1	1	0	1	1	1	0	1	1	0	0	2077.233	0.013	2077.246
9	0	0	0	1	0	0	0	1	1	0	1	0	2349.174	-0.032	2349.141
10	1	2	0	0	2	0	0	0	3	1	0	1	2548.343	0.024	2548.367
11	0	4	2	0	1	2	2	0	2	0	0	1	2586.546	0.039	2586.585
12	2	0	0	0	2	0	0	0	2	1	1	0	2671.144	0.000	2671.144
13	0	4	4	0	0	4	4	0	1	0	0	0	2677.936	0.049	2677.985
14	1	2	2	0	1	2	2	0	1	1	0	0	2762.269	0.018	2762.287
15	1	2	0	0	2	0	0	0	1	1	0	1	2797.157	-0.020	2797.137
16	0	1	1	1	0	1	1	1	1	0	1	0	3004.453	-0.058	3004.395
17	1	3	1	0	2	1	1	0	3	1	0	1	3181.792	0.062	3181.854
18	0	5	3	0	1	3	3	0	2	0	0	1	3244.101	0.045	3244.146
19	2	1	1	0	2	1	1	0	2	1	1	0	3339.706	0.040	3339.746
20	0	5	5	0	0	5	5	0	1	0	0	0	3350.284	0.058	3350.343
21	1	3	3	0	1	3	3	0	1	1	0	0	3445.706	0.030	3445.735
22	1	3	1	0	2	1	1	0	1	1	0	1	3501.033	0.030	3501.063
23	0	2	0	1	1	0	0	1	2	0	1	1	3612.891	-0.052	3612.839
24	0	2	2	1	0	2	2	1	1	0	1	0	3660.884	-0.073	3660.811
25	1	0	0	1	1	0	0	1	1	2	0	0	3714.852	-0.071	3714.781
26	1	4	0	0	3	0	0	0	4	1	0	2	3792.656	0.027	3792.683
27	1	4	2	0	2	2	2	0	3	1	0	1	3823.531	0.046	3823.577
28	0	6	4	0	1	4	4	0	2	0	0	1	3904.544	0.045	3904.589
29	3	0	0	0	3	0	0	0	3	1	2	0	3942.517	0.025	3942.542
30	2	2	2	0	2	2	2	0	2	1	1	0	4009.441	0.035	4009.476
31	0	6	6	0	0	6	6	0	1	0	0	0	4023.775	0.061	4023.836
32	3	0	0	0	3	0	0	0	2	1	2	0	4064.277	-0.002	4064.275
33	1	4	4	0	1	4	4	0	1	1	0	0	4128.500	0.036	4128.536
34	1	4	2	0	2	2	2	0	1	1	0	1	4198.897	0.026	4198.923
35	1	4	0	0	3	0	0	0	1	1	0	2	4225.111	-0.014	4225.097
36	0	3	1	1	1	1	1	1	2	0	1	1	4248.131	-0.044	4248.088
37	0	3	3	1	0	3	3	1	1	0	1	0	4318.455	-0.070	4318.386
38	1	1	1	1	1	1	1	1	1	2	0	0	4391.058	-0.046	4391.012
39	1	5	1	0	3	1	1	0	4	1	0	2	4416.480	0.061	4416.541
40	1	5	3	0	2	3	3	0	3	1	0	1	4470.630	0.034	4470.665
41	0	7	5	0	1	5	5	0	2	0	0	1	4567.381	0.036	4567.417
42	3	1	1	0	3	1	1	0	3	1	2	0	4591.448	0.060	4591.508
43	0	0	0	2	0	0	0	2	1	1	1	0	4673.371	-0.049	4673.322
44	2	3	3	0	2	3	3	0	2	1	1	0	4680.274	0.037	4680.311
45	0	7	7	0	0	7	7	0	1	0	0	0	4698.403	0.055	4698.458
46	3	1	1	0	3	1	1	0	2	1	2	0	4753.794	0.048	4753.841
47	1	5	5	0	1	5	5	0	1	1	0	0	4811.138	0.037	4811.175
48	1	2	0	1	2	0	0	1	3	2	0	1	4853.681	-0.060	4853.622
49	0	4	2	1	1	2	2	1	2	0	1	1	4889.592	-0.062	4889.531
50	1	5	3	0	2	3	3	0	1	1	0	1	4893.567	0.030	4893.597
51	1	5	1	0	3	1	1	0	1	1	0	2	4938.732	0.044	4938.775
52	0	4	4	1	0	4	4	1	1	0	1	0	4977.178	-0.065	4977.113
53	2	0	0	1	2	0	0	1	2	3	0	0	4977.889	-0.056	4977.833
54	1	6	0	0	4	0	0	0	5	1	0	3	5022.354	-0.002	5022.352
55	1	6	2	0	3	2	2	0	4	1	0	2	5048.803	0.023	5048.825
56	1	2	2	1	1	2	2	1	1	2	0	0	5063.368	-0.051	5063.317
57	1	2	0	1	2	0	0	1	1	2	0	1	5099.731	-0.072	5099.659
58	1	6	4	0	2	4	4	0	3	1	0	1	5121.776	0.013	5121.788
59	3	2	0	0	4	0	0	0	4	1	2	1	5197.228	0.026	5197.255
60	0	8	6	0	1	6	6	0	2	0	0	1	5232.314	0.019	5232.333

Figure 1. Blue circles: Average ro-vibrational errors for 337 vibrational ($J = 0$) states from HITRAN estimated as CO$_2$ $\tilde{E}_\lambda^{\mathrm{H}} - \tilde{E}_\lambda^{\mathrm{T}}$ (HITRAN-TROVE) term values for $J \leqslant 40$, which were used as band centre corrections (see text). Red crosses: Average residuals for the ro-vibrational CO$_2$ term values (for $J \leqslant 40$) between TROVE (before the band centre correction) and calculations from Zak et al. (2016) using DVR3D and the same PES Ames-2016 for 294 vibrational states.

3 LINE LIST

3.1 Quantum numbers

In TROVE calculations, the ro-vibrational states are uniquely identified by three numbers, the rotational angular momentum quantum number J, the total symmetry Γ (Molecular symmetry group) and the eigen-state counting number λ (in the order of increasing energies). Each state can be further assigned with approximate quantum numbers (QN) associated with the corresponding largest basis set contribution (Yurchenko et al. 2007). There are two main sets of approximate QNs corresponding to the contractions steps 1 and 3. The first set is connected to the primitive basis set excitation numbers v_1, v_2, v_3 and l_2. The second set is associated with the vibrational counting number λ from the ($J = 0$)-contracted basis set Eq. (5). Even though v_1, v_2, v_3 and l_2 are more physically intuitive than the counting number of the vibrational states λ, the latter is useful for correlating TROVE's states to the experimental (e.g. normal mode) QNs or indeed to any other scheme. Table 1 shows vibrational ($J = 0$) term values of CO$_2$ together with all assignment schemes either used in these work or relevant to the spectroscopy of CO$_2$: (i) TROVE primitive QNs v_1, v_2, v_3 and l, (ii) TROVE band centres counting number λ, (iii) HITRAN QNs m_1, m_2, l_2, m_3, r adopted for CO$_2$ and (iv) spectroscopic (normal mode) QNs $n_1, n_2^{\mathrm{lin}}, l_2, n_3$ used for other general linear triatomic molecules. Our preferred choice is (iv). According to this convention, n_1 and n_3 are two stretching quantum numbers associated with the symmetric and asymmetric modes; n_2^{lin} is the (symmetric) linear molecule bending quantum number; l_2 is the bending quantum number satisfying the standard conditions on the vibrational angular momentum of an isotropic 2D Harmonic oscillator (Bunker & Jensen 1998)

$$l_2 = n_2^{\mathrm{lin}}, n_2^{\mathrm{lin}} - 2, \ldots 1(0).$$

All ro-vibrational states are automatically assigned the QN schemes (i) and (ii), which were then automatically correlated to the general linear molecule QN (iv) using the following rules:

$$l = l_2, \quad v_1 + v_2 = n_1 + n_3, \quad v_3 = n_2^{\mathrm{lin}},$$

for a given stretching polyad $n_1 + n_2$, where we assumed that the asymmetric quanta has higher energies than symmetric. For example, for $v_1 + v_2 = n_1 + n_3 = 2$ the stretching QNs (n_1, n_3) and assigned to the vibrational term values according

with the order of energies: $(2,0)$ 3339.702 cm^{-1}, $(1,1)$ 3714.853 cm^{-1} and $(0,2)$ 4673.392 cm^{-1}. The linear molecule bending quantum number n_2^{lin} is given by

$$n_2^{\text{lin}} = 2v_3 + l_2,$$

where v_3 is the TROVE vibrational bending quantum number. The standard linear molecule QN scheme (iv) was favoured for example by Herzberg & Herzberg (1953) and is also recommended here.

We could not perform similar automatic correlation to the HITRAN quantum labels (m_1, m_2, l_2, m_3, r) for all the states in our line lists, only for states present in the CO$_2$ HITRAN database. The HITRAN convention of quantum numbers (iii) for CO$_2$ is more empirical. It is motivated by energy clusters formed by states in accidental Fermi resonance and their order within a cluster (Rothman & Young 1981). The quantum number m_1 is associated with Fermi resonance groups of (symmetric) states of different combinations of l_2 and $2m_1 + m_2 = 2n_1 + n_2^{\text{lin}}$; r is the ranking index, with $r = 1$ for the highest vibrational level of a Fermi resonance group and assuming the values $1, 2, \ldots m_1 + 1$ (Rothman & Young 1981). HITRAN's version of the bending quantum number m_2 is by definition equal to l_2 (so-called AFGL notation) and thus redundant, while the stretching quantum number m_3 is the same as the linear molecule asymmetric quantum number n_3 from scheme (iv). In order to simplify correlation with HITRAN and experimental literature, the scheme (iii) is retained, but only for the ro-vibrational states present in HITRAN.

4 LINE LIST

The CO$_2$ UCL-4000 line list contains 3 480 477 states and 2 557 551 923 transitions and covers the wavenumber range from 0 to 20 000 cm^{-1} (wavelengths, $\lambda > 0.5$ μm) with the lower energy up to 16 000 cm^{-1} and $J \leqslant 202$ with a threshold on the Einstein coefficients of 10^{-14} s^{-1}. The line list consists of two files (Tennyson et al. 2016), called States and Transitions, which in the case of UCL-4000 are summarised in Tables 2 and 3. The first 4 columns of the States file have the compulsory structure for all molecules: State ID, Energy term value (cm^{-1}), the total degeneracy and the total angular momentum. According to the new ExoMol-2020 format (Tennyson et al. 2020), the 5th column is also compulsory representing the uncertainty estimate of the corresponding term value (cm^{-1}), which is followed by the lifetime, Landé g-factor (if provided) and molecular specific quantum numbers, including rigorous (symmetry, parity) and non-rigorous (vibrational, rotational, etc). The States file covers all states up to $J = 230$ (3 526 057 states). The Transitions part consists of three columns with the upper State ID, lower State ID and the Einstein A coefficient, see Table 3. For convenience, the Transition part is split into 20 files each covering 1000 cm^{-1}.

The uncertainty of the CO$_2$ energies were estimated based on the two main criteria. For the states matched to and replaced by the HITRAN energies, the uncertainties σ (in cm^{-1}) are taken as the HITRAN errors of the corresponding line positions as specified by the HITRAN error codes (Rothman et al. 2005). For all other states the following conservative estimate is used:

$$\sigma = 0.01\, n_1 + 0.01\, n_2^{\text{lin}} + 0.01\, n_3.$$

With the lower state energy threshold of 16 000 cm^{-1} our line list should be valid for temperatures up to at least 2500 K. Figure 2 (left) illustrates the effect of the lack of the population for the states higher than 16 000 cm^{-1} with the help of the CO$_2$ partition function $Q(T)$. In this figure we show a ratio of incomplete $Q^{E_{\max}}(T)$ (using only states below $E_{\max}$) over 'complete' Q^{36000}(T). This ratio has the difference of 2 % for Q^{16000} at $T = 2500$ K and Q^{26000} at $T = 4000$ K, which are the estimates for maximal temperature of the line list for wavenumber regions 0–20 000 cm^{-1} and 10 000–20 000 cm^{-1}, respectively. In Figure 2 (right) we compare the partition functions of CO$_2$ computed using our line list with the Total Internal Partition Sums (TIPS) values for CO$_2$ (Gamache et al. 2017). The energies in our line list cover higher rotational excitations ($J_{\max} = 230$) compared to TIPS, which was based on the threshold of $J_{\max} = 150$. The energy thresholds in both cases are comparable, $hc \cdot 36\,000$ cm^{-1} vs $hc \cdot 30\,383$ cm^{-1} (TIPS). The threshold value of $J_{\max} = 150$ corresponds the energy term value of $\sim 10\,000$ cm^{-1} and thus leads the underestimate of the partition function of high T, while with the threshold of $J_{\max} = 230$ all states below 20 000 cm^{-1} are included.

In order to improve the calculated line positions, CO$_2$ energies from HITRAN were used to replace the TROVE energies where available, taking advantage of the two-part structure of the UCL-4000 line list consisting of a States file and Transition files (Tennyson et al. 2016). A HITRAN energy list consisting of 18 392 empirical values from 337 vibrational states covering J values up to 129 was generated by collecting all lower and upper state energies from the ^{12}C^{16}O$_2$ HITRAN transitions. Comparison of the calculated TROVE term energies with these 18 668 HITRAN values gives an rms error of 0.016 cm^{-1} and is illustrated in Fig. 3 in a log-scale.

The overview of the CO$_2$ absorption spectrum and its temperature dependence are illustrated in Fig. 4. CO$_2$ has a prominent band at 4.3 μm, commonly used for atmospheric and astrophysical retrievals. For example, it was used as one of the photometric bands for the Spitzer Space Telescope (Werner et al. 2004).

Our line list is designed to almost perfectly agree with the HITRAN line positions, which was achieved by replacing the
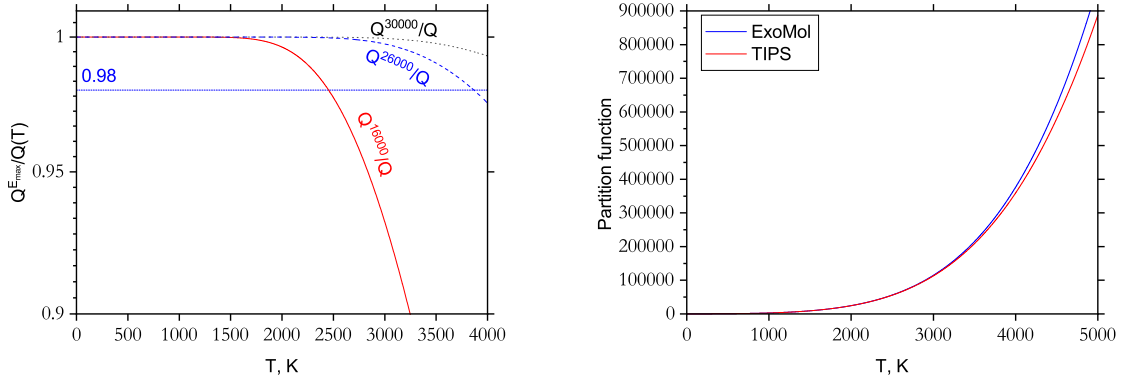
Table 2. Extracts from the final states file for UCL-4000.

i	$\tilde{E}$	g_{tot}	J	unc.	Γ	e/f	n_1	n_2^{lin}	l_2	n_3	C_i	m_1	m_2	m_3	m_4	r	v_1^{T}	v_2^{T}	v_3^{T}
1	0.000000	1	0	0.0005	A1	e	0	0	0	0	1.00	0	0	0	0	1	0	0	0
2	1285.408200	1	0	0.0005	A1	e	0	2	0	0	1.00	1	0	0	0	2	0	0	1
3	1388.184200	1	0	0.0050	A1	e	1	0	0	0	1.00	1	0	0	0	1	1	0	0
4	2548.366700	1	0	0.0005	A1	e	1	2	0	0	1.00	2	0	0	0	3	1	0	1
5	2671.142957	1	0	0.0050	A1	e	2	0	0	0	1.00	2	0	0	0	2	1	1	0
6	2797.136000	1	0	0.0050	A1	e	1	2	0	0	1.00	2	0	0	0	1	1	0	1
7	3792.681898	1	0	0.0050	A1	e	1	4	0	0	1.00	3	0	0	0	4	1	0	2
8	3942.541358	1	0	0.0050	A1	e	3	0	0	0	1.00	3	0	0	0	3	1	2	0
9	4064.274256	1	0	0.0050	A1	e	3	0	0	0	1.00	3	0	0	0	2	1	2	0
10	4225.096148	1	0	0.0050	A1	e	1	4	0	0	1.00	3	0	0	0	1	1	0	2
11	4673.325200	1	0	0.0005	A1	e	0	0	0	2	1.00	0	0	0	2	1	1	1	0
12	5022.349428	1	0	0.0050	A1	e	1	6	0	0	1.00	4	0	0	0	5	1	0	3
13	5197.252900	1	0	0.0050	A1	e	3	2	0	0	1.00	4	0	0	0	4	1	2	1
14	5329.645446	1	0	0.0050	A1	e	4	0	0	0	1.00	4	0	0	0	3	2	2	0
15	5475.553054	1	0	0.0005	A1	e	3	2	0	0	1.00	4	0	0	0	2	1	2	1
16	5667.644584	1	0	0.0050	A1	e	2	4	0	0	1.00	4	0	0	0	1	1	1	2
17	5915.212302	1	0	0.0005	A1	e	0	2	0	2	1.00	1	0	0	2	2	1	1	1
18	6016.690121	1	0	0.0005	A1	e	1	0	0	2	1.00	1	0	0	2	1	0	3	0
19	6240.044061	1	0	0.08	A1	e	2	6	0	0	1.00	-1	-1	-1	-1	-1	1	1	3
20	6435.507278	1	0	0.06	A1	e	4	2	0	0	1.00	-1	-1	-1	-1	-1	2	2	1
21	6588.323819	1	0	0.05	A1	e	5	0	0	0	1.00	-1	-1	-1	-1	-1	3	2	0
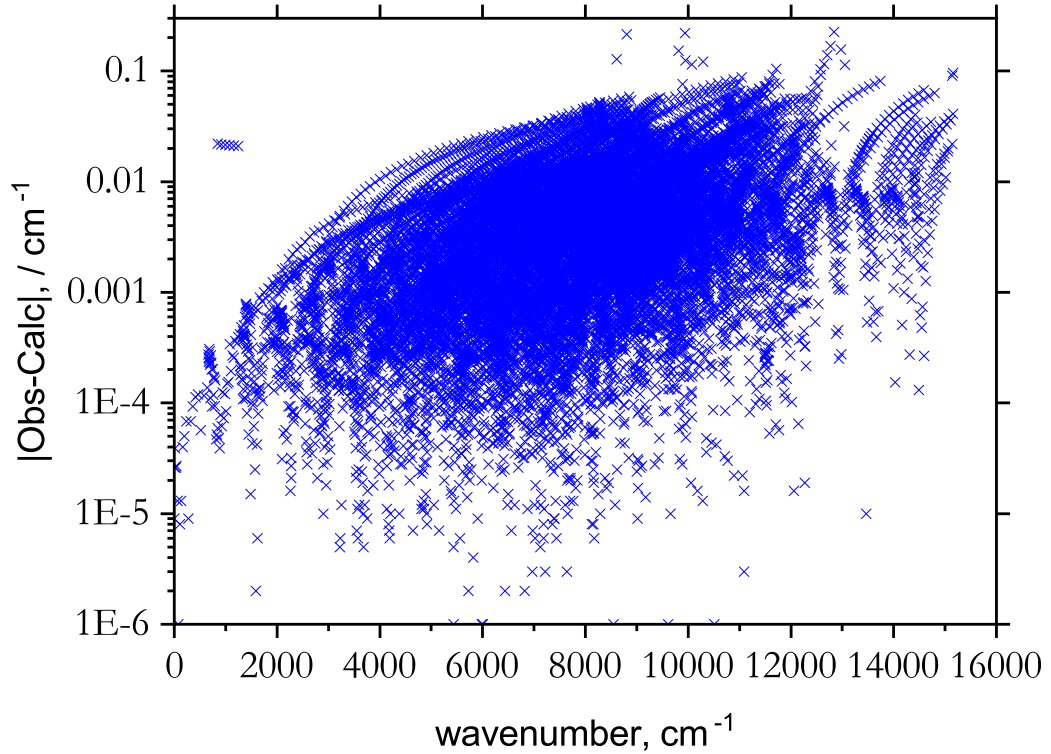
i: State counting number.
$\tilde{E}$: State energy in cm^{-1}.
g_{tot}: Total state degeneracy.
J: Total angular momentum.
unc.: Uncertainty cm^{-1}: The empirical (4 decimal places) and estimated (2 decimal places) values.
Γ: Total symmetry index in $\mathcal{C}_{2\text{v}}(\text{M})$
e/f: Kronig rotationless parity
n_1: Normal mode stretching symmetry (A_1) quantum number.
n_2^{lin} : Normal mode linear molecule bending (A_1) quantum number.
l_2: Normal mode vibrational angular momentum quantum number.
n_3: Normal mode stretching asymmetric ($B1_1$) quantum number.
C_i: Coefficient with the largest contribution to the ($J = 0$) contracted set; $C_i \equiv= 1$ for $J = 0$.
m_1: CO$_2$ symmetric vibrational Fermi-resonance group quantum number (-1 stands for non available).
m_2: CO$_2$ vibrational bending quantum number (similar but not exactly identical to n_2^{lin}).
l_2: CO$_2$ vibrational bending quantum number (similar but not exactly identical to standard l_2).
m_3: CO$_2$ asymmetric vibrational stretching quantum number, the same as n_3.
r: CO$_2$ additional ranking quantum number identifying states within a Fermi-resonance group.
v_1^{T}: TROVE stretching vibrational quantum number.
v_2^{T}: TROVE stretching vibrational quantum number.
v_3^{T}: TROVE bending vibrational quantum number.

Table 3. Extract from the transitions file for the UCL-4000 line list.

f	i	A_{fi}
1176508	1137722	2.8564E-02
1861958	1849078	1.6327E-03
631907	665295	8.1922E-12
1344897	1331267	4.2334E-07
983465	944281	1.4013E-08
183042	170520	1.6345E-02
2695389	2668685	5.9366E-07
811518	822542	1.4353E-01
406949	369902	2.3774E-02

f: Upper state counting number.
i: Lower state counting number.
A_{fi}: Einstein-A coefficient in s^{-1}.
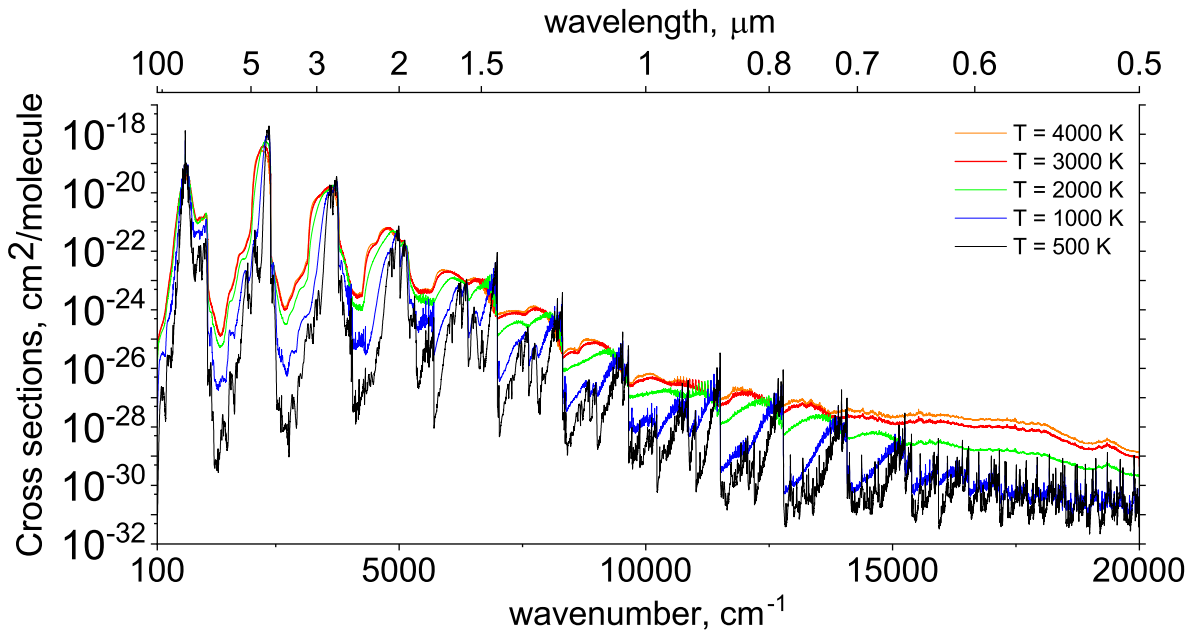
Figure 2. Partition functions of CO_2. Left display: Ratio $Q^{E_{max}}(T)/Q(T)$ of the CO_2 partition functions at with energy cutoffs $hc \cdot 16\,000$ cm^{-1}, $hc \cdot 26000$ cm^{-1} and $hc \cdot 30000$ cm^{-1}, as a function of temperature. $Q(T)$ is chosen as $Q^{36000 \text{ cm}^{-1}}$. The line 0.98 shows that the recommended temperature varies with the wavenumber region, from $T = 2500$ K (> 0 cm^{-1}) to $T = 4000$ K ($> 10\,000$ cm^{-1}). Right display: ExoMol values were computed using all UCL-4000 energies for $J \leqslant 230$; TIPS values were obtained using the TIPS app provided in Gamache et al. (2017).
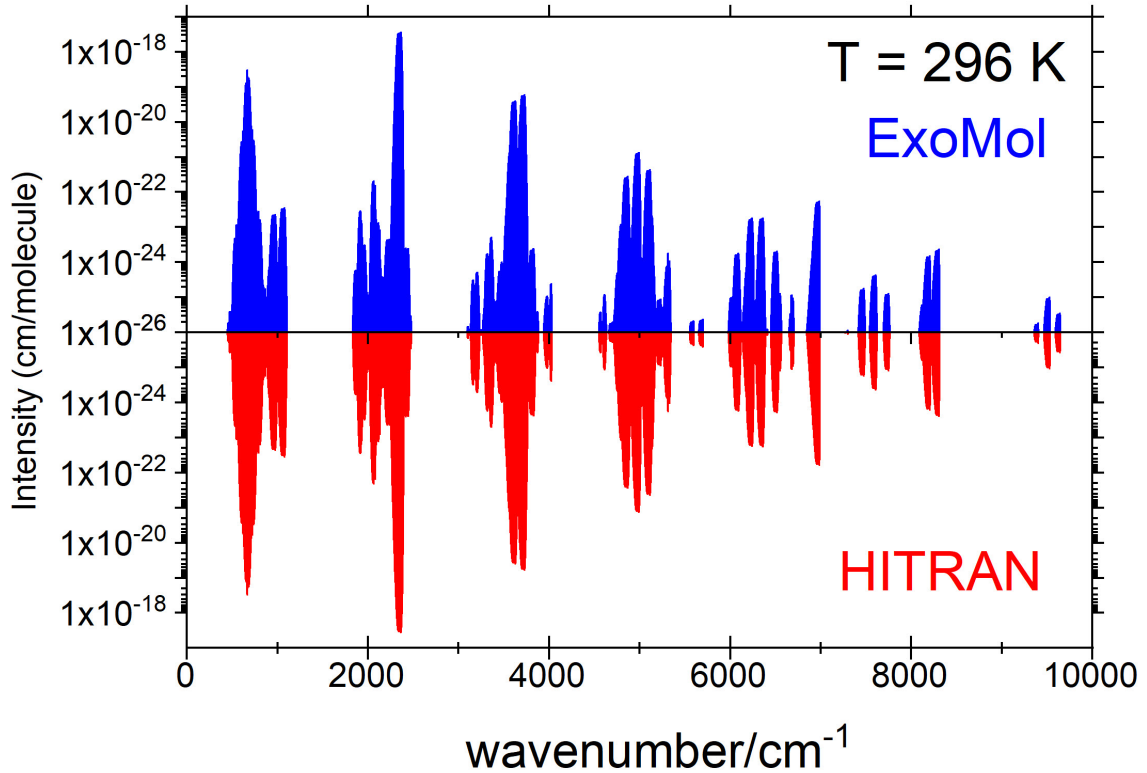
Figure 3. Ro-vibrational Obs.-Calc. errors $|\tilde{E}_i^{\text{H}} - \tilde{E}_i^{\text{T}}|$ (HITRAN-TROVE) in cm^{-1} for all HITRAN's 18 392 empirical values as a function of the energy term values, covering $J \leqslant 129$ giving an rms error of 0.016 cm^{-1}.

TROVE energies with the energies collected from the HITRAN data set for CO_2. Figures 5 and 6 offer some comparisons with HITRAN. In turn, the accuracy of the line intensities agree well with the HITRAN values as guaranteed by the quality of the UCL *ab initio* DMS used. The mean ratio of our intensities to HITRAN is 1.0029 with the standard error of 0.00029 for 171143 HITRAN lines we could establish a correlation to.
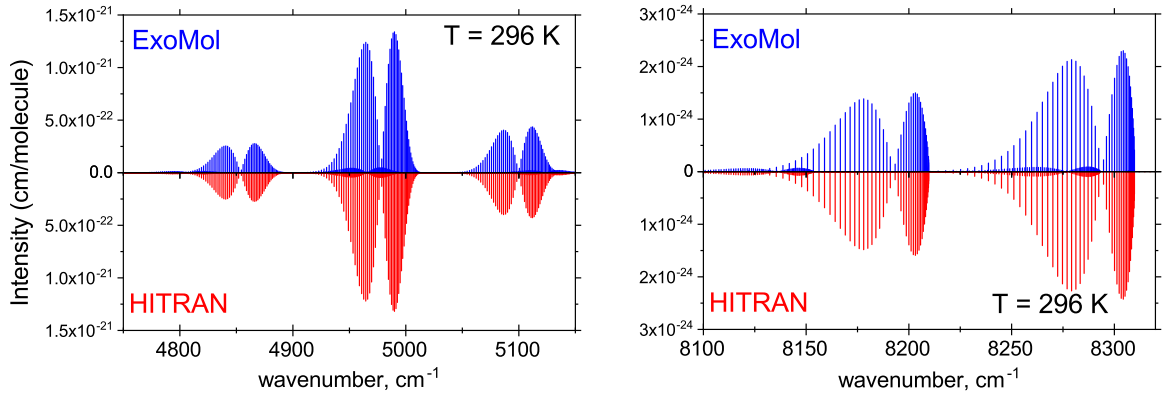
Figure 7 compares the performance of the four main line lists for hot CO_2, UCL-4000 (this work), CDSD-4000 (effective Hamiltonian) (Tashkun & Perevalov 2011), Ames-2 (variational) (Huang et al. 2017) and 2010 HITEMP (empirical) (Rothman et al. 2010) for the wavenumber range from 0 to 15 000 cm^{-1}. In general the UCL-4000 line list gives the highest opacity at
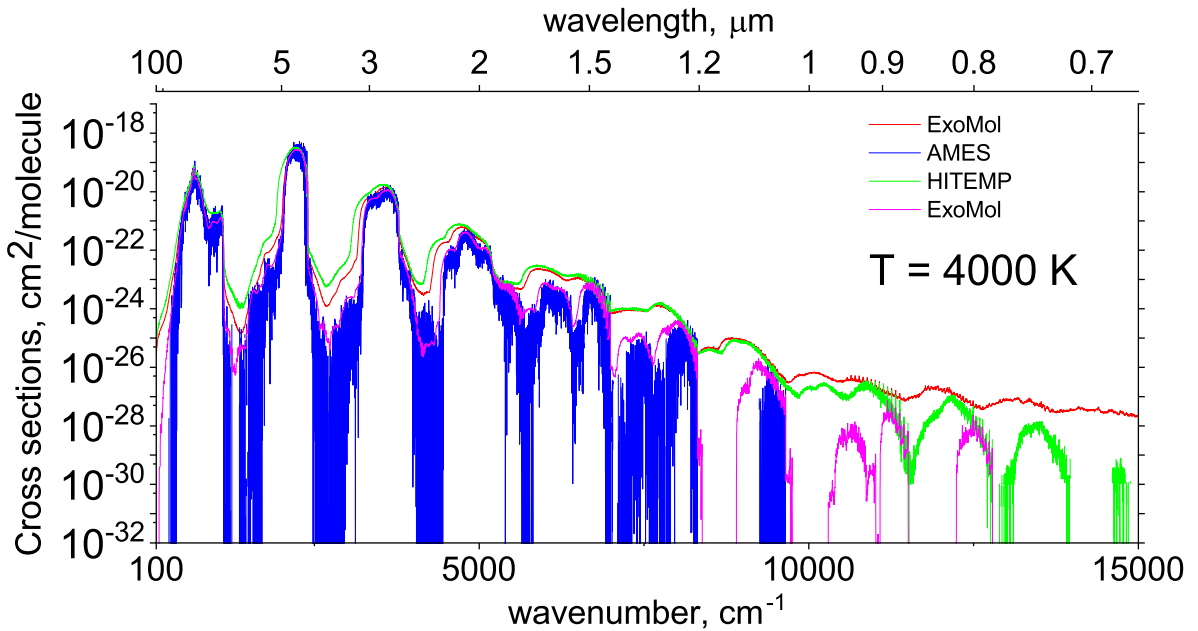
Figure 4. Temperature dependence of the CO$_2$ spectrum using the Gaussian line profile of HWHM=1 cm^{-1}. The spectrum becomes systematically flatter with increasing temperature.

Figure 5. CO$_2$ stick spectrum comparing using UCL-4000 to HITRAN at $T = 296$ K.

Figure 6. Absorption stick spectrum of CO_2 computed using UCL-4000 and compared to HITRAN at $T = 296$ K for two spectroscopic regions.
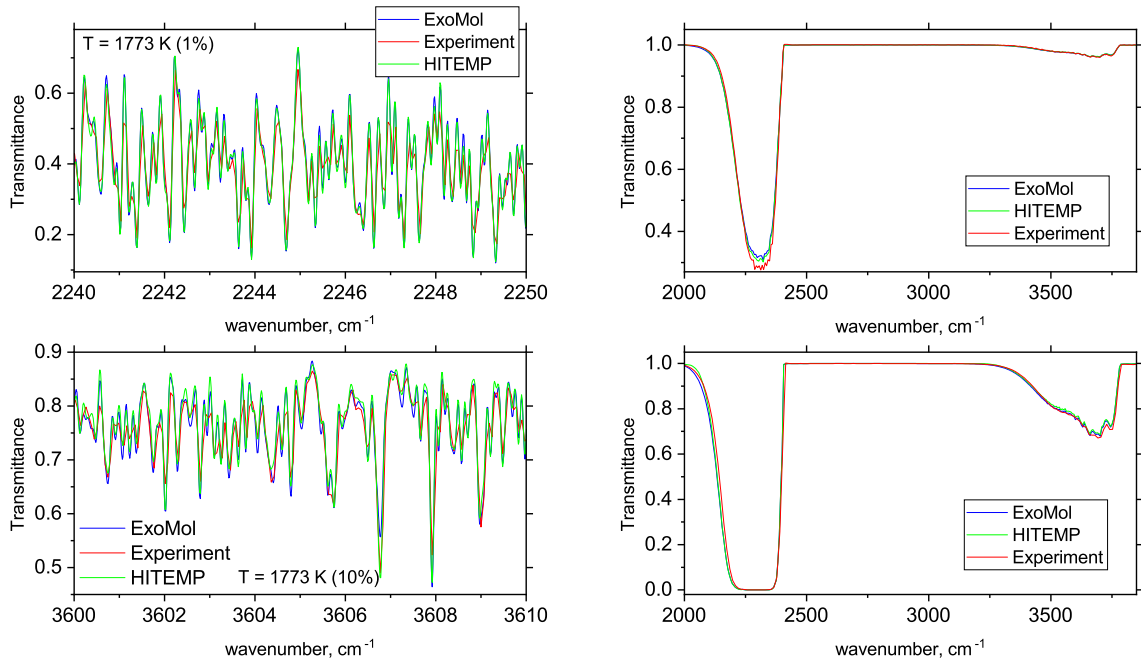

Figure 7. Comparing UCL-4000, CDSD-4000 (Tashkun & Perevalov 2011), Ames-2016 (Huang et al. 2017) and 2010 HITEMP (Rothman et al. 2010) spectra of CO_2 at $T = 4000$ K. A Gaussian line profile of HWHM=1 cm^{-1} was used in each case.

$T = 4000$ K which is due to its being more complete, while both CDSD-4000 and 2010 HITEMP omit too many hot bands to be able to compete with the other two line lists at high T. The Ames-2016 line list also lacks a significant portion of the opacity at short wavelengths at this temperature as expected from the low energy threshold used (Huang et al. 2017).

Figure 8 compares the UCL-4000 spectrum of CO_2 at $T = 1773$ K with the experiment by Evseev et al. (2012), who recorded transmittance of CO_2 at the normal pressure. The displays on the left show small windows from the two strongest CO_2 bands, 2.7 μm and 4.3 μm at higher resolution, while the displays on the right gives an overview of the whole region covering these bands at lower resolution. As a reference, spectra computed with the 2010 HITEMP line list are also shown. At this temperature, UCL-4000 performs very similarity to 2010 HITEMP and shows excellent agreement with the experiment.

5 CONCLUSION

A new hot line list for the main isotopologue of CO_2 ($^{12}C^{16}O_2$) is presented, which is the most comprehensive (complete and accurate) data set for carbon dioxide to date. The line list is an important addition to the ExoMol database which now contains line lists for all the major constituents of hot Jupiter and mini-Neptune exoplanets. Line lists are still being added to address the problem of hot super Earth exoplanets, or lava planets, the composition of whose atmospheres are currently not well constrained.

Figure 8. Comparing HITEMP and ExoMol to experimental transmittance (Evseev et al. 2012) at $T = 1773$ K and 1 bar using a Voigt profile. The experiments were performed with 1% (upper) and 10% (lower) CO_2 in N_2 buffer gas. HITEMP line width parameters were used for HITEMP, while for UCL-4000 we used an approximate scheme a0 from the ExoMol diet (Barton et al. 2017) based on the HITRAN values. The left display shows two selected windows at high resolution (0.0125 cm^{-1}), while the right display is with broader overview and lower resolution (6 cm^{-1}).

The line lists can be downloaded from the CDS (http://cdsweb.u-strasbg.fr/) or from ExoMol (www.exomol.com) databases.

DATA AVAILABILITY STATEMENT

Full data is made available. The line lists can be downloaded from the CDS (http://cdsweb.u-strasbg.fr/) or from ExoMol (www.exomol.com databases.

The complete list of the band centres and their corrections is given as supplementary material to the paper

REFERENCES

Barton E. J., Hill C., Czurylo M., Li H.-Y., Hyslop A., Yurchenko S. N., Tennyson J., 2017, J. Quant. Spectrosc. Radiat. Transf., 203, 490

Baylis-Aguirre D. K., Creech-Eakman M. J., Güth T., 2020, MNRAS, 493, 807

Bunker P. R., Jensen P., 1998, Molecular Symmetry and Spectroscopy, 2nd edn. NRC Research Press, Ottawa

Carter S., Handy N., Sutcliffe B., 1983, Mol. Phys., 49, 745

Chubb K. L., Tennyson J., Yurchenko S. N., 2020, MNRAS, 493, 1531

12

Connor B. et al., 2016, Atmos. Meas. Tech., 9, 5227

Cooley J. W., 1961, Math. Comp., 15, 363

Evseev V., Fateev A., Clausen S., 2012, J. Quant. Spectrosc. Radiat. Transf., 113, 2222

Gamache R. R. et al., 2017, J. Quant. Spectrosc. Radiat. Transf., 203, 70

Gordon I. E., et al., 2017, J. Quant. Spectrosc. Radiat. Transf., 203, 3

Heng K., Lyons J. R., 2016, ApJ, 817, 149

Herzberg G., Herzberg L., 1953, J. Opt. Soc. Am., 43, 1037

Hougen J. T., Bunker P. R., Johns J. W. C., 1970, J. Mol. Spectrosc., 34, 136

Huang X., Freedman R. S., Tashkun S. A., Schwenke D. W., Lee T. J., 2013, J. Quant. Spectrosc. Radiat. Transf., 130, 134

Huang X., Gamache R. R., Freedman R. S., Schwenke D. W., Lee T. J., 2014, J. Quant. Spectrosc. Radiat. Transf., 147, 134

Huang X., Schwenke D. W., Freedman R. S., Lee T. J., 2017, J. Quant. Spectrosc. Radiat. Transf., 203, 224

Huang X., Schwenke D. W., Lee T. J., 2019, J. Quant. Spectrosc. Radiat. Transf., 230, 222

Huang X., Schwenke D. W., Tashkun S. A., Lee T. J., 2012, J. Chem. Phys., 136, 124311

Kang P., Wang J., Liu G.-L., Sun Y. R., Zhou Z.-Y., Liu A.-W., Hu S.-M., 2018, J. Quant. Spectrosc. Radiat. Transf., 207, 1

Long D., Reed Z., Fleisher A., Mendonca J., Roche S., Hodges J., 2020, Geophys. Res. Lett., 47, e2019GL086344

Massol H. et al., 2016, Space Sci. Rev., 205, 153

Medvedev E. S., Meshkov V. V., Stolyarov A. V., Ushakov V. G., Gordon I. E., 2016, J. Mol. Spectrosc., 330, 36

Medvedev E. S., Ushakov V. G., Conway E. K., Upadhyay A., Gordon I. E., Tennyson J., 2020, J. Quant. Spectrosc. Radiat. Transf., 252, 107084

Moses J. I., Madhusudhan N., Visscher C., Freedman R. S., 2013, ApJ, 763, 25

Noumerov B. V., 1924, MNRAS, 84, 592

Odintsova T., Fasci E., Moretti L., Zak E. J., Polyansky O. L., Tennyson J., Gianfrani L., Castrillo A., 2017, J. Chem. Phys., 146, 244309

Oyafuso F. et al., 2017, J. Quant. Spectrosc. Radiat. Transf., 203, 213

Polyansky O. L., Bielska K., Ghysels M., Lodi L., Zobov N. F., Hodges J. T., Tennyson J., 2015, Phys. Rev. Lett., 114, 243001

Rein K. D., Sanders S. T., 2010, Appl. Optics, 49, 4728

Rothman L. S. et al., 2010, J. Quant. Spectrosc. Radiat. Transf., 111, 2139

Rothman L. S. et al., 2005, J. Quant. Spectrosc. Radiat. Transf., 96, 139

Rothman L. S., Young L. D., 1981, J. Quant. Spectrosc. Radiat. Transf., 25, 505

Snels M., Stefani S., Grassi D., Piccioni G., Adriani A., 2014, Planet Space Sci., 103, 347

Sutcliffe B. T., Tennyson J., 1991, Int. J. Quantum Chem., 39, 183

Swain M. R. et al., 2010, Nature, 463, 637

Swain M. R. et al., 2009a, ApJ, 704, 1616

Swain M. R., Vasisht G., Tinetti G., Bouwman J., Chen P., Yung Y., Deming D., Deroo P., 2009b, ApJL, 690, L114

Tashkun S. A., Perevalov V. I., 2011, J. Quant. Spectrosc. Radiat. Transf., 112, 1403

Tashkun S. A., Perevalov V. I., Teffo J. L., Bykov A. D., Lavrentieva N. N., 2003, J. Quant. Spectrosc. Radiat. Transf., 82, 165

Tennyson J., Kostin M. A., Barletta P., Harris G. J., Polyansky O. L., Ramanlal J., Zobov N. F., 2004, Comput. Phys. Commun., 163, 85

Tennyson J., Yurchenko S. N., 2012, MNRAS, 425, 21

Tennyson J. et al., 2020, J. Quant. Spectrosc. Radiat. Transf.

Tennyson J. et al., 2016, J. Mol. Spectrosc., 327, 73

Vargas J., Lopez B., da Silva M. L., 2020, J. Quant. Spectrosc. Radiat. Transf., 245, 106848

Čermák P., Karlovets E. V., Mondelain D., Kassi S., Perevalov V. I., Campargue A., 2018, J. Quant. Spectrosc. Radiat. Transf., 207, 95

Wattson R. B., Rothman L. S., 1992, J. Quant. Spectrosc. Radiat. Transf., 48, 763

Werner M. W. et al., 2004, ApJS, 154, 1

Yurchenko S. N., Barber R. J., Tennyson J., 2011, MNRAS, 413, 1828

Yurchenko S. N., Mellor T. M., 2020, J. Chem. Phys., submitted

Yurchenko S. N., Thiel W., Jensen P., 2007, J. Mol. Spectrosc., 245, 126

Yurchenko S. N., Yachmenev A., Ovsyannikov R. I., 2017, J. Chem. Theory Comput., 13, 4368

Zak E. J., Tennyson J., Polyansky O. L., Lodi L., Tashkun S. A., Perevalov V. I., 2016, J. Quant. Spectrosc. Radiat. Transf., 177, 31

Zak E. J., Tennyson J., Polyansky O. L., Lodi L., Zobov N. F., Tashkun S. A., Perevalov V. I., 2017a, J. Quant. Spectrosc. Radiat. Transf., 203, 265

Zak E. J., Tennyson J., Polyansky O. L., Lodi L., Zobov N. F., Tashkun S. A., Perevalov V. I., 2017b, J. Quant. Spectrosc. Radiat. Transf., 189, 267